PROCEEDINGS, 48th Workshop on Geothermal Reservoir Engineering
Stanford University, Stanford, California, February 6-8, 2023
SGP-TR-224

Geology, State of Stress, and Heat in Place for a Horizontal Well Geothermal Development Project at Blue Mountain, Nevada

Steven FERCHO[1], Jack NORBECK[1], Emma MCCONVILLE[1], Nick HINZ[2], Irene WALLIS[2], Aleksei TITOV[1], Saurabh AGARWAL[1], Sireesh DADI[1], Christian GRADL[1], Hank BACA[1], Eric EDDY[1], Camden LANG[1], Katharine VOLLER[1], and Timothy LATIMER[1]

[1]Fervo Energy, 100 North Arlington Avenue, Suite 320, Reno, Nevada 89501, United States

Steve@FervoEnergy.com

[2]Geologica Geothermal Group, 75 Caliente St, Reno, Nevada 89509, United States

Keywords: Near-Field EGS, Horizontal Drilling, Proppant, Heat in Place, State of Stress

ABSTRACT

Fervo Energy is developing a commercial nearfield enhanced geothermal system project adjacent to the Blue Mountain geothermal field, located in northern Nevada. The goal of the project is to provide production uplift to the Blue Mountain power facility, as well as to demonstrate the efficacy of Fervo's horizontal geothermal well design and reservoir management strategy. In this paper, we present the geologic conceptual model that formed the basis for targeting a three-well drilling campaign, which included Vertical Monitoring Well 73-22, Horizontal Injection Well 34A-22, and Horizontal Production Well 34-22, three deep wells that were drilled and completed successfully in 2022. In addition, we present key data used to constrain the state of stress and geomechanical model at the Blue Mountain site, including laboratory measurements on core samples, image logs, and petrophysical logs. Well prognoses were developed from geologic, thermal, and conceptual hydrothermal models based on available data prior to the drilling of these new wells. We then compare the geologic prognoses for all three wells against the as-drilled lithology and temperature profiles. Based on the updated geologic model following the successful drilling campaign, we estimated the heat in place and power capacity for this project.

The project area intentionally targeted the hot (350 °F to 400 °F) and low-permeability, thermally conductive margins of the active hydrothermal system to demonstrate the feasibility of horizontal drilling and multistage stimulation in geothermal formations and at high-temperature conditions. The horizontal wells were strategically oriented to balance stable temperature along the laterals with optimal orientation to the local stress field. Three-dimensional temperature modeling and analysis of drilling induced fractures from offset well image logs successfully informed the well placements.

The lithologies encountered at the target depths of the laterals were Mesozoic metasediments composed of interlayered phyllite and quartzite intruded by diorite and granodiorite dike swarms. Drilling results from Vertical Monitoring Well 73-22, which targeted a location approximately at the midpoint of the laterals, confirmed the predicted temperatures and depth to Mesozoic basement, which informed the drilling program of the subsequent horizontal wells. The equilibrated temperature profiles of the horizontal wells were measured by both wireline logging and fiber optic sensing equipment installed permanently behind the casing in both wells. Following the stimulation treatment in Injection Well 34A-22, Production Well 34-22 was drilled through the stimulated reservoir volume. Acoustic and resistivity image logs were obtained along the lateral of Production Well 34-22, and we observed numerous fractures aligned with the maximum horizontal stress orientation suggesting the presence of tensile fractures created during the stimulation treatment. In addition, proppant samples were detected at numerous locations while drilling the lateral section of Horizontal Production Well 34-22, suggesting that proppant injected during the stimulation treatment on Injection Well 34A-22 was transported significant distances away from the wellbore. Heat-in-place estimates confirm that the stimulated reservoir volume created from the stimulation treatment in well 34A-22 was sufficiently large to enable approximately 5 MW of electric power production over a 10-year project life, consistent with the target well performance for the horizontal doublet geothermal well system.

1. INTRODUCTION

In this paper we present the geology and temperature results from a first of its kind geothermal horizontal well development completed by Fervo Energy (Fervo). Three-dimensional geologic and temperature models were built from a synthesis of the existing data, new geologic mapping, and reassessment of existing well logs. We describe the models and results that led to the successful targeting and drilling of Fervo's three wells at the site, which include a vertical monitoring well and two horizontal wells that define an injection and production well pair. Data gained on both the regional and local state of stress was gathered to inform targeting of the lateral wells. The orientation of the horizontal portions of Fervo wells 34A-22 and 34-22 was informed by balancing the known orientation of the stress field to keep the laterals perpendicular to the direction of maximum horizontal stress (SH_{max}) while targeting to maintain relatively consistent temperature along the laterals informed by the 3D temperature model. As each well was drilled, the 3D geologic and temperature models described in this paper were used as a basis for pre-drill prognoses, and then the models were iteratively updated with actual results. After the drilling phase was completed, two heat in place models were created to describe the exploitable energy located between the Fervo horizontal wells and within the larger stimulated reservoir volume created around the Fervo horizontal wells.

2. GEOLOGIC MODEL

Previous studies of Blue Mountain define that the overall stratigraphic framework consists of Miocene to present basin-fill deposits overlying Mesozoic phyllite. The phyllite is intruded by multiple phases of igneous dikes/sills of likely Mesozoic and Tertiary ages. The range-front fault on the SW side of the Blue Mountain forms a prominent topographic break. On the NW side of Blue Mountain, silicified fault breccia is locally exposed in isolated outcrops surrounded by alluvium along the westernmost exposures of the surface trace of this fault (Figure 1). As previously noted by Szybinski (2005) and in later reports, the westernmost exposure of this fault zone is silicified, and the silicification was interpreted to be relict. Kinematic data collected from fault surfaces along the western half of the range-front fault indicate dextral-oblique motion. Quaternary fault scarps were not observed in the alluvium along this range-front fault, supporting that either this fault has not ruptured since the middle Pleistocene and scarps are no longer preserved, or if younger scarps are present, they are subtle and might only be mapped with Lidar, a dataset which has not been available for this resource area

New mapping of the Blue Mountain field was undertaken for Fervo by Geologica Geothermal Group (Geologica) as part of a 2020 Resource Evaluation Report (Geologica, 2020). This work determined that the western nose of the Blue Mountain range is cut by multiple subparallel strands of arcuate normal and dextral-normal faults that splay from the range-front fault on the SW side of the range and wrap around to the range-front fault system on the northwest side of the range. There is also relatively widespread argillic alteration and localized silicification in the same area. One of these faults is particularly prominent, distinguished by massive silicification of fault breccia (Figure 1) along all exposures of the fault zone in the Mesozoic metasediments spanning 1.5 km in length along strike. It is possible that the silicification continues northward, but the fault trace is only exposed displacing Quaternary surficial sediments. Two fault dip measurements were acquired along separate segments with dips of 61 to 68° E. The gentler of the two dipping surfaces also had good quality kinematic indicators, indicating dextral-normal offset on a NW-striking segment. This Silicified Fault Zone corresponds to the Central fault on the map by Szybinski (2005), who also noted the extensive silicification. Based on field assessment in this study, there was no Quaternary fault scarp associated with this fault that cuts alluvium. There is, however, a sharp topographic break that is above the elevation of the Lake Lahontan high stand. This escarpment could be related to middle Pleistocene faulting or could be related to differential erosion across the Silicified Fault core.

Several faults were mapped east of the Silicified Fault Zone described above (Figure 1). One corresponds partly with the East fault mapped by Szybinski (2005). Silicification was not observed along this fault zone. The trace is based partly on some offset dikes and Mesozoic bedding offsets (Szybinski, 2005; this study) and partly on a major topographic break between the main range and a bench which extends west to the Silicified Fault previously described. The topographic break is consistent with an early to middle Pleistocene fault scarp. A possible late Pleistocene Quaternary fault scarp was also noted cutting alluvial fan sediments along a fault segment (Figure 1) between the East and Central faults as mapped by Szybinski (2005).

Several fault strands were mapped west of the Silicified Fault, and in the West fault area of Szybinski (2005). Fault drag is locally observed in the Mesozoic strata, with relative counterclockwise rotation of the Mesozoic fabric within 5 to 20 meters of some fault segments west of the Silicified Fault Zone. The exposures are erosion modified by the high stand of Lake Lahontan and it is difficult to determine which, if any have Quaternary fault scarps. Most of the WNW-striking sinistral faults and the NE-striking thrust faults mapped in the western part of the Blue Mountain range by Szybinski (2005) could not be confirmed. NE-trending ridges are present, but these were interpreted by Geologica (2020) as erosional hogbacks with the primary bedding in the phyllite parallel to these ridges. The overall expression of the range-front fault system on the NW side of the Blue Mountain range is different from the range-front on the south side in that it consists of multiple sub-parallel Quaternary-active strands covering an area 1-2 km wide (Figure 1). In the area near Blue Mountain Well 89-11, six parallel fault strands were mapped with fault scarps in the alluvium. One or two of these displace lacustrine sediments below the Lake Lahontan high stand, others are truncated by the shorelines. Fault surfaces were measured on several fault surfaces exposed in phyllite.

Based on the map pattern of the faults and kinematic data, the Blue Mountain geothermal system is associated with a displacement transfer zone (e.g., Faulds and Hinz, 2015). In this structural model, the range-front along the SW side of the range is dextral-normal. This fault dies out into the basin west of the nose of the range and dextral shear is transferred to NE-striking normal faults that accommodate NW-SE extension in the form of pure dip-slip motion along the NW side of the Blue Mountain range. In this type of model, deep circulation would most likely be controlled by the N to NE-striking normal faults, near where they intersect the NW-striking dextral-normal fault system. This could include faults associated with the relict alteration exposed at the surface and/or concealed faults in the basin. At the surface, a number of these fault segments are associated with relict alteration of Pliocene to early Quaternary age, a pattern which is relatively common for faults controlling deep circulation geothermal systems in the Basin and Range province.

In order to better understand the subsurface and help with targeting of Fervo's wells at Blue Mountain, a faulted 3D geologic model was created by combining the new Geologica surface mapping with data on lithologies, losses, and drilling breaks from the mudlogs from existing deep wells (Figure 2). The stratigraphic framework for the 3D model consists of Triassic metasediments that are intruded by Miocene (~12ma) diorite dikes and overlain by late Tertiary through Quaternary basin fill sediments. For the basis of updating the 3D geologic model, the Triassic metasediments and Tertiary intrusives are lumped as one basement unit (Mz), and the late Cenozoic basin-fill sediments are lumped into a second unit (QTs).

As is the case in most extensional settings, the wells located furthest out in the basin have the deepest depth to basement, especially 13-11 and 41-27 which are idle wells on the northern and southern margins of the field. The rest of the infield and nearfield wells show less variance in depth to basement as a function of distance to the range-front because faulting within the field is controlling the lithologic contacts. Stratigraphic control from the well data shows that the basement progressively steps down to the NW, with the contact within each fault block gently dipping back towards the range front. This classic Basin-and-Range style faulting is best demonstrated in section A (Figure 3). The NW, N, and NE -striking faults which drop basement down in the core of the field are truncated to the south by the SW

range front fault, which strikes from SE to NW across the SW side of Blue Mountain and continues obscured under basin fill to the west. On the north end of the field, these core faults merge into the NW range front of Blue Mountain.

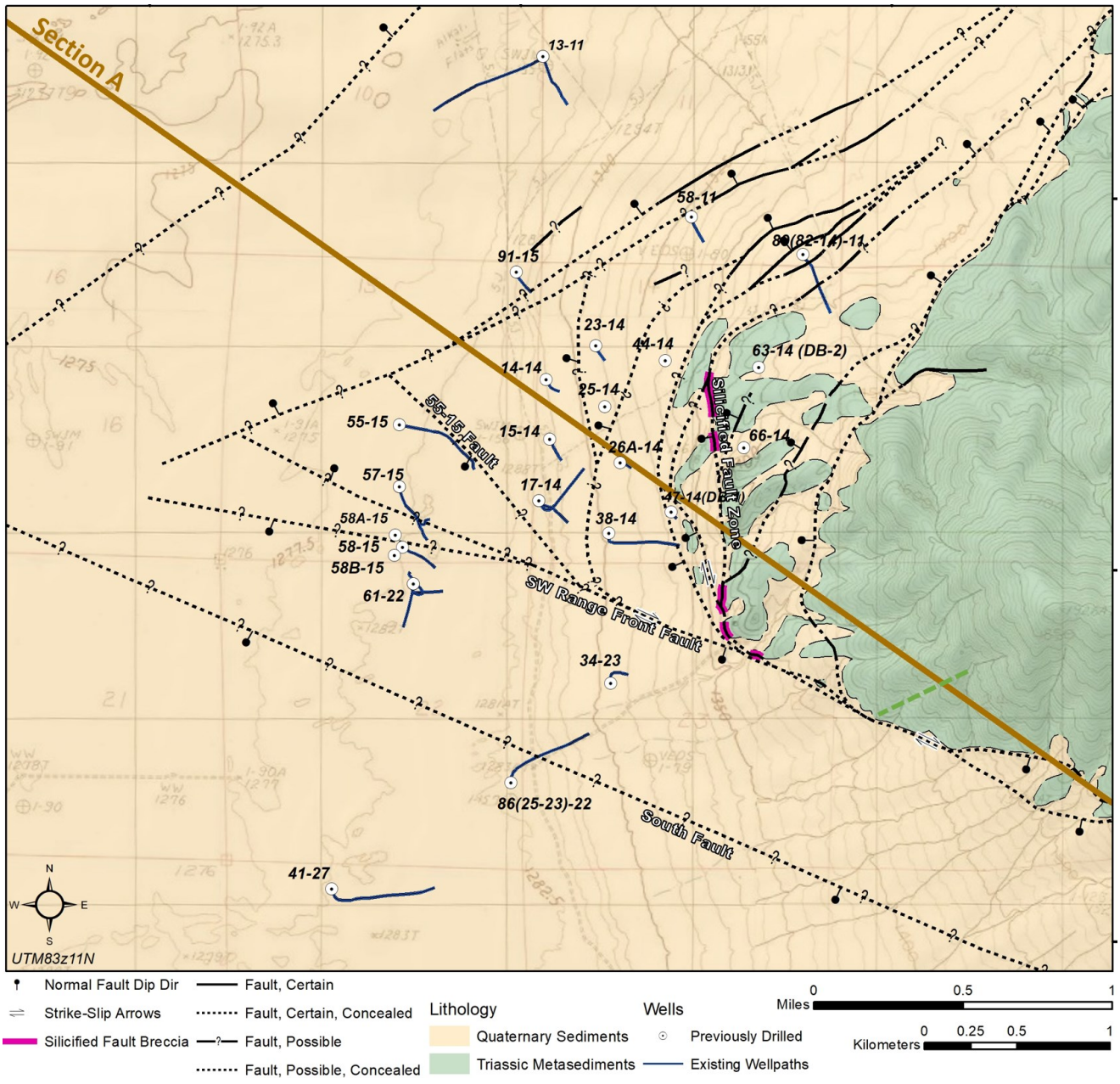

Figure 1: Geologic and structural map of the Blue Mountain Field including previously drilled deep wells.

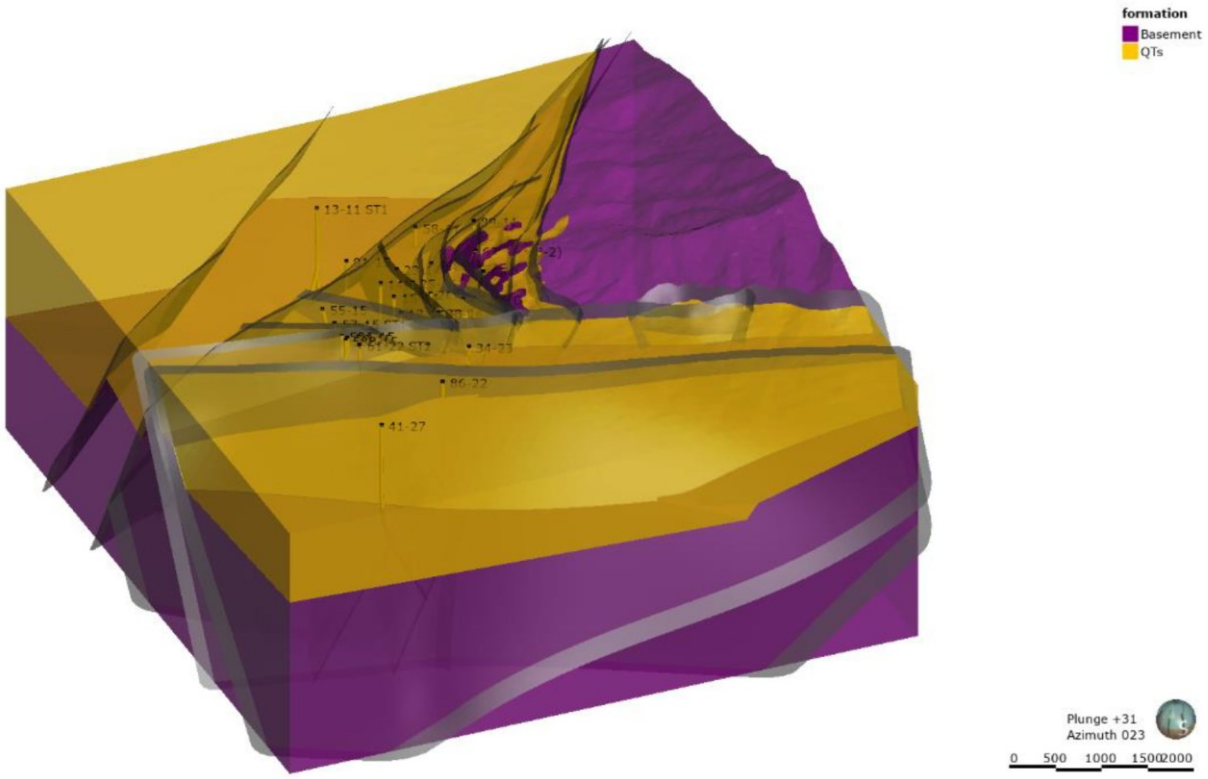

Figure 2: Oblique view of the Blue Mountain three-dimensional geologic model.

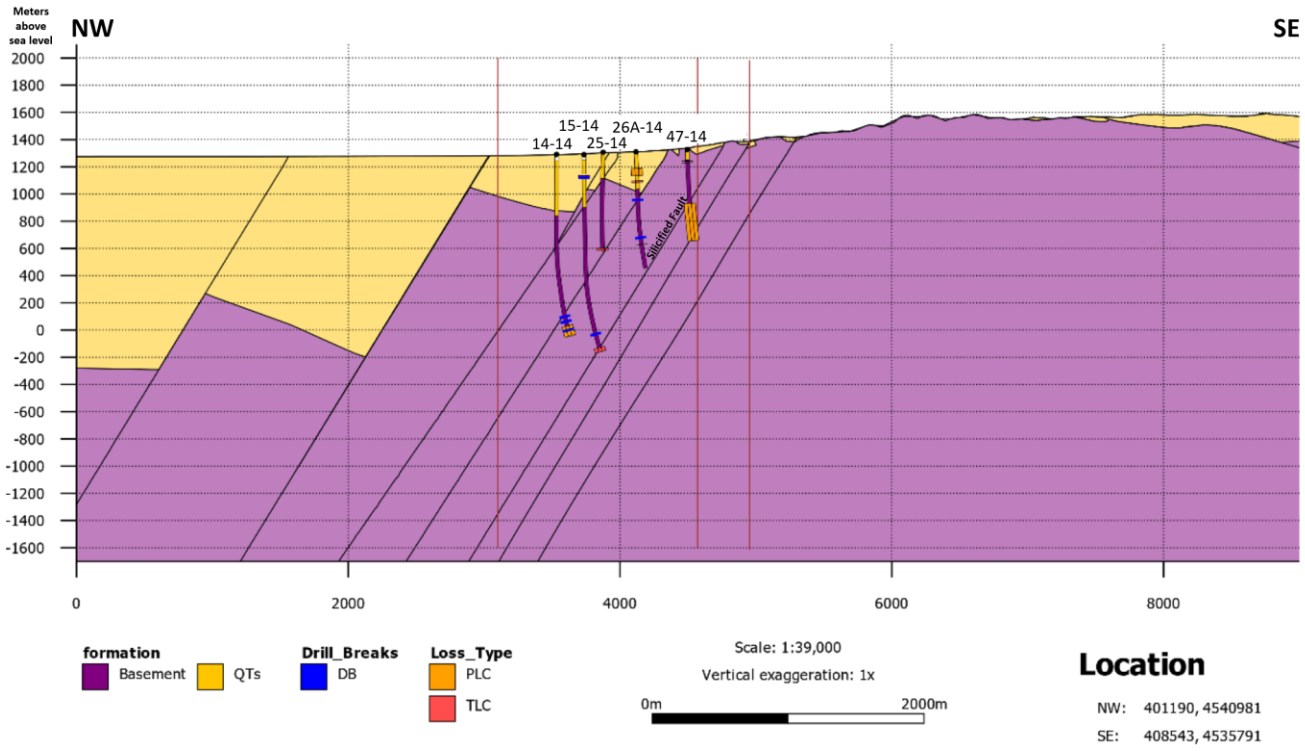

Figure 3: Cross Section A, position shown in Figure 1. Stratigraphic control from the well data shows that the basement progressively steps down to the NW, with the contact within each fault block gently dipping back towards the range front.

3. TEMPERATURE MODEL

The available temperature logs for deep wells at Blue Mountain were plotted against elevation to normalize changes in measured depth due to directional drilling and to also be able to evaluate temperatures across common aquifers. The coolest wells in the field are 41-27, 13-11, 86-22, and 34-23, and have conductive profiles with gradients around 45°C/km (3.4°F/100 ft). This gradient corresponds to the average conductive gradient for the upper 3 km in the Basin and Range province (Coolbaugh et al., 2005). These wells can be considered outside the convective geothermal system and provide useful information in defining background conditions for the field. The remaining wells have higher initial gradients ranging from 60-200˚C/km (4.3-12.0°F/100 ft) followed by abrupt changes to below 30˚C/km (2.6°F/100 ft), characteristic of when wells enter partially convecting geothermal systems. Wells 63-14 and 38-14 both exhibit strong temperature reversals after reaching 160-180°C (320-356˚F), indicative of outflow from the hydrothermal system. The hottest wells in the field are 57-15 and 58-15, with the latter having a maximum measured temperature of 218°C (424°F) and increasing gradient at bottom indicating the upflow may be 225°C (437°F) or more.

A 3D temperature model was created by importing the static temperature logs to the Leapfrog Geothermal software and plotted along the directional well tracks (Figure 4). Three-dimensional interpolation of the temperatures was completed using the software's Radial Basis Function (RBF). RBF is an algorithm widely used for implicit surface modelling modeling and is well adapted for temperature distribution modeling. An initial raw model was created considering only measured temperature values as inputs and letting the RBF naturally contour temperatures in increments of 25°C. These were then projected to the cross sections (matching geology section locations) which were used to review the model and draw 2D interpretive contours where needed that honor static well temperature data and make thermodynamic corrections for areas between and beyond the wells. Additionally, control points were added along the boundaries of the model to enforce a uniform 45°C/km (3.4°F/100 ft) background gradient around the model edges. These 2D control contours and control points were integrated into the 3D temperature model so that both the temperature interpretations and the static temperature points along the well bores were incorporated.

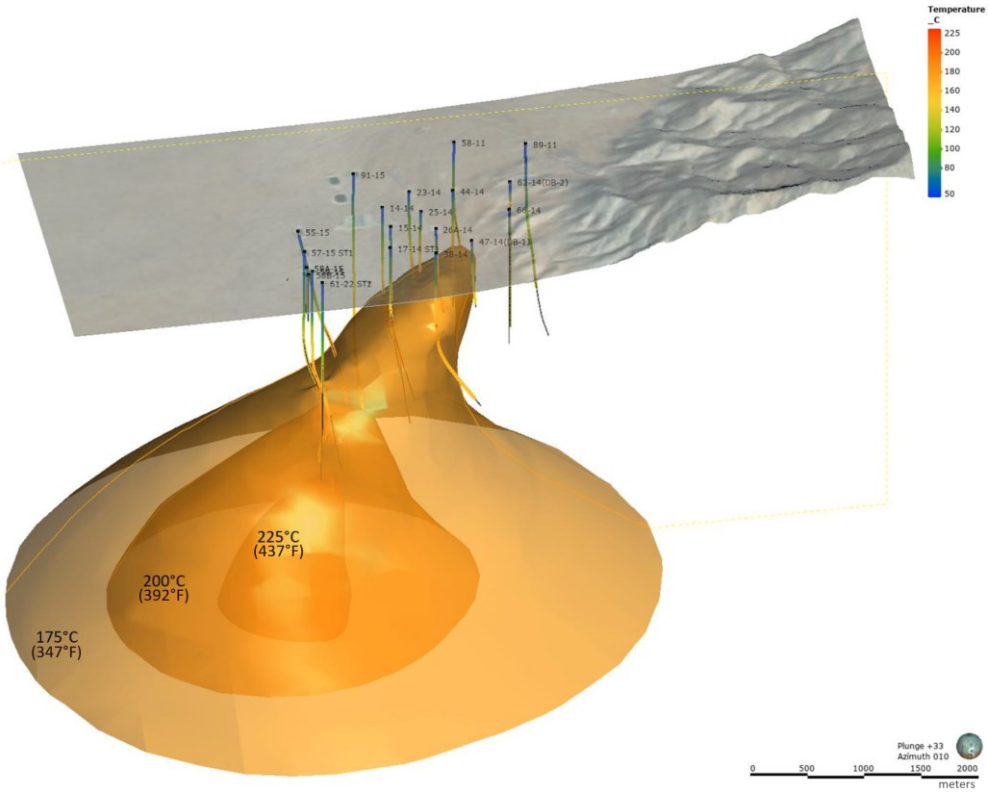

Figure 4: Oblique view looking NNE at the highest temperature contours of the 3D temperature model of Blue Mountain.

In the resulting conceptual model, upflow primarily rises along the NNW-striking Silicified Fault Zone from deep basement formation in the west towards the surface trace of the fault at the eastern edge of the field (Figure 5). At the ground surface, the alteration is relict, and it was not clear based only on the surface expression that this fault zone was going to correlate with inferred fluid flow pathways through the reservoir until the conceptual model was completed. Fluid upflow with temperatures greater than 225°C (437°F) rises along the Silicified Fault Zone below and to the west of the 57-15 and 58-15 well pads where wells recorded a maximum measured temperature of 218 °C (424°F). The high temperature gradients of both wells at total depth suggest greater than 225°C (437°F) is likely to be present within a few hundred meters of the bottom of these wells. This upflow temperature is consistent with geothermometry from well DB-1, in which reservoir fluids have chalcedony geothermometer reporting ~220°C (428°F) and cation geothermometry reporting approximately

235-250 °C (455-482°F) (Niggemann et al., 2005). The >225+°C upflow along the Silicified Fault Zone likely has a narrow chimney geometry, given that wells 61-22 and 55-15 are substantially cooler to either side of 58-15 and 57-15 (Figure 5). Wells 58-15, 57-15, and 61-22 do not intersect the main trace of the Silicified Fault Zone and just miss the main upflow below, but do likely intersect a major synthetic fault in the hanging wall of the main fault. The upflow chimney likely follows a key structural perturbation along the Silicified Fault, such as an intersection with a splay of the SW range-front fault, or a small step in the fault zone. Given the limitations of geophysical modeling and that image logs have not been collected in wells 61-22, 58-15, and 57-15, these possible options for local fault zone complexities cannot be effectively evaluated at this time.

The 200+°C (392°F) upflow continues to rise east from below the pads for wells 58-15 and 57-15 where upflow ascends nearly due east toward the well 17-14 area, whereby it turns NE and 175-200°C (347-392°F) fluids continue to 58-11. The outflow depth and breadth are best depicted by the flow arrows shown in Figure 5. Along the upflow path, several hanging walls and maybe one footwall splay may carry some of the fluids as interpreted from well temperature curves. South of the geothermal upflow and outflow zones at Blue Mountain there have been a handful of wells previously drilled (86-22, 41-27, and 34-23) which exhibit relatively conductive temperature conditions and lack deep permeability or connectivity to the rest of the wellfield. This permeability boundary along the south side of the reservoir lies just south of well 61-22 and has been interpreted to be associated with the down-dip projection of the southwest range-front fault (Figure 5). This recognized lack of deep permeability, reservoir connectivity, and elevated conductive temperatures radiating from the active system to the north makes the southern field (south of green line in Figure 5) relatively compartmentalized, and therefore an ideal testbed for Fervo's horizontal well program.

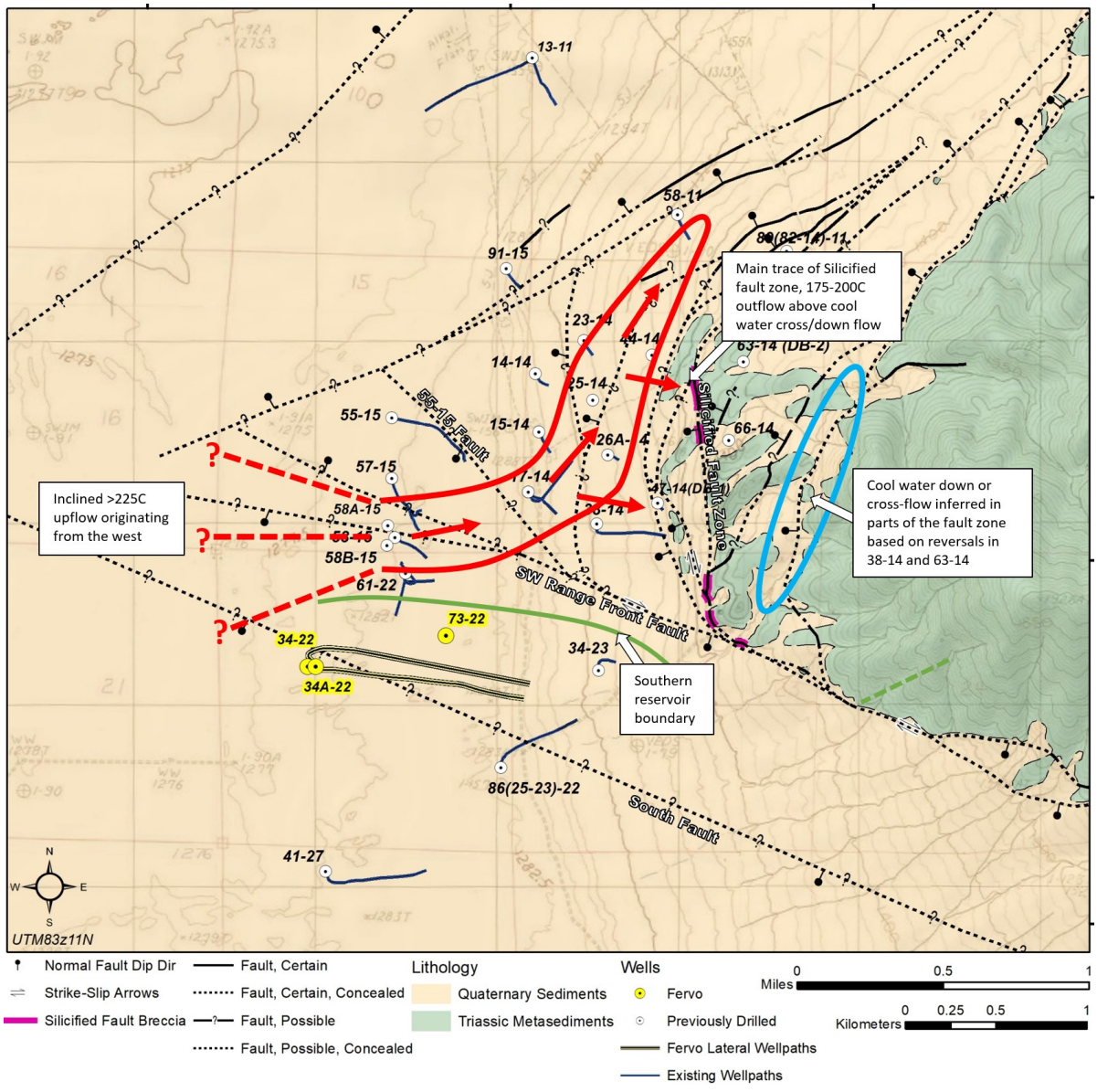

Figure 5: Geology and wellfield map showing the conceptual model, including an approximate southern boundary of the convective geothermal reservoir, and the placement of Fervo's wells (highlighted in yellow).

4. GEOLOGY AND TEMPERATURE RESULTS OF FERVO WELLS

Fervo chose the area south of well 61-22 (Figure 5) to target its enhanced horizontal well program due to known relatively high temperatures and a lack of deep permeability or reservoir connectivity described in Section 3. Fervo targeted and drilled three deep wells in this southern reservoir area, starting with the vertical observation well 73-22 which was designed to test the depth to Mesozoic basement and temperature model at a position midway through the laterals which Fervo subsequently planned to drill. Well 73-22 was also outfitted with permanent DAS (distributed acoustic sensing) and DTS (distributed temperature sensing) fiber to serve as a monitoring station for the future drilling, stimulation, and production of Fervo's lateral wells. After drilling well 73-22, Fervo targeted and drilled the horizontal injection well 34A-22 to a depth of 11,220 ft MD (7,664 ft TVD) and then the horizontal production well 34-22 to a depth of 11,225 ft MD (7,524 TVD). The orientation of the horizontal portions of wells 34A-22 and 34-22 was informed by balancing the known orientation of the stress field (see Section 5) to keep the laterals normal to SH_{max} while trying to maintain relatively consistent temperature along the laterals informed by the 3D temperature model. As each well was drilled, the 3D geologic model and temperature models described in this paper were used as a basis for pre-drill prognoses, and then the models wee iteratively updated with actual results.

4.1 Observation Well 73-22

Fervo first tested the southern low-permeability/high temperature area by drilling the vertical 73-22 monitoring well at the horizontal mid-point of the Fervo lateral wells (34-22 and 34A-22) which were planned to be drilled following completion of 73-22. In addition to having the purpose of serving as a monitoring well outfitted with permanent acoustic and temperature sensing fiber for Fervo's pilot project, 73-22 also had a major de-risking function of further defining the top phyllite basement contact depth, identification of fault hazards, and depth to temperature Fervo's temperature target of 350°F.

The predicted temperature curve for 73-22 shown in Figure 6 was derived by placing the planned well path in the 3D temperature model and projecting temperatures onto the wellbore. After completion of drilling 73-22, a permanent temperature/pressure sensor was installed in the well at 7,920 ft measured depth (MD) and provided a near-equilibrium reading of 368.5°F. The original model for 73-22 predicted a temperature of 360°F at 7,920 ft MD, which is 8.5°F cooler than actual measured temperature. DTS fiber was also installed in 73-22 and provides a full temperature depth profile of the well. After correction of the DTS fiber curve to match the installed 7,920' P/T sensor, the curve shown in Figure 24 was obtained. The calibrated DTS temperatures were also confirmed later with an equilibrated wireline temperature log. The DTS curve follows the shape of the predicted model but is 7-15°F warmer than predicted, and more isothermal below a depth of around 5,000 ft MD. The temperature perturbations between 500 ft MD and 1000 ft MD are likely caused by near-wellbore fluid flow through fractures in the silicified sediments where the well had shallow lost circulation through silicified sediments. The DTS curve also shows a small rollover or cooling of reservoir temperature of a few degrees F between 6,000 ft MD and 7,000 ft MD.

The pre-drill geologic model described in Section 2 predicted 73-22 would contact the phyllite basement at a depth of 2,075 ft MD, and error bars were included extending uncertainty from 1,600-2,400 ft MD based on the lack of existing wells for >1,300 ft horizontally in any direction around the well. While drilling 73-22, the phyllite was encountered at a depth of 2,410 ft MD, just at the edge of the deep pre-drill error bar. To update the geologic model based on this deeper result, it was observed that Cyrq well 34-23 to the east and Fervo 73-22 make a relatively straight line pointing down in the direction of the phyllite bedding dip as observed at surface. Connecting the phyllite contacts between Cyrq 34-23 and Fervo 73-22, a dip of 32° to the east is achieved. The previous dip assumption on the contact in this fault block was 29° to the east. This update of dip angle deepened the basement contact prediction for the future Fervo 34A-22 well to 3,750 ft MD (3,500-4,000 ft error bars). The previous estimate of the contact for 34A-22 using the pr-drilling 3D geologic model was 3,000' with 2,600-3,400 ft error bars.

Four potential fault zones were identified in the 73-22 pre-drill prognosis based on the initial 3D model. The faults in the vicinity of 73-22 dip towards south the west, making the 73-22 vertical well location ideal to de-risk the faults for where they would have potentially intersected deeper in Fervo's future planned lateral wells. Two of the four predicted faults were ranked as low probability as they were thought to terminate north of 73-22. There is evidence that the SW Range Front Fault was encountered in the form of a zone of silicic breccia and calcite mineralization observed from 4,250-4,340 ft MD a short period of 50 bbl/hr starting at 4,330 ft MD which quickly was healed by loss circulate materials (LCM) and cuttings. The two low probability faults were not observed, and neither was the final moderate probability fault (55-15 Fault). It is possible that 55-15 fault has a slightly higher dip angle than was modeled and therefore may still exist below the total depth (TD) of 8,009 ft MD of 73-22 rather than at 7,550 ft MD projected depth based on a shallower dip.

A significant zone of shallow silicified sediments were observed in 73-22. Silicified sediments are formed when silica enriched geothermal fluids outflow through permeable sands and gravels and deposit an extremely hard matrix surrounding the sand, clay, and gravel grains. They cause slow drilling rate, are abrasive to the bit and drill strings, and most importantly, lead to a total loss of circulation (TLC) of the drilling fluids. TLC was observed in nearly all the offset wells at Blue Mountain while or drilling through silicified sediment zones, and therefore they were identified in Fervo's pre-drilling analysis as a key hazard and indicator of TLC. To prepare for this hazard, Fervo set up a reliable and continuous water supple to drill "blind" when the silicified sediment zone and losses occurred, and a geologic monitoring program to alert key rig personnel when the silicified sediments were observed in cuttings. Well 73-22 ended up encountering the silicified sediments at a depth of ~550 ft MD and drilled through them to a depth of 992 ft MD where circulation was lost. The well was successfully drilled blind with reserve water supply until returns were regained temporarily from 1,006 to 1,073 ft MD likely due to a plugging off the loss zone with cuttings, before another fracture within the silicified sediments accompanied by a large drilling break encountered at 1,073 ft MD led to total loss of circulation again. Two cement plugs were spotted to try to cure losses in this zone, but TLC persisted until returns were slowly regained to 100% at a depth of 1,545 ft MD. The regaining of circulation may have been contributed to by a combination of the cement and packing off the fracture with hundreds of feet of cuttings.

Figure 6: Pre-Drill temperature predictions versus actual measured temperatures for Fervo's three wells at Blue Mountain

4.2 Injection Well 34A-22

The predicted temperature profile for 34A-22 shown on Figure 6 was derived from the 3D temperature model after updates with the results from Fervo's 73-22 monitoring well. In 34A-22, 7-in completion casing was cemented from TD to surface with DTS fiber on June 2nd, and DTS monitoring has been ongoing since. The latest DTS temperature profile for the well shows a very similar shape to what was predicted, with a perfect match to predicted 368°F at the heel (8000 ft MD) and 340°F at the toe (11,000 ft MD) where 348°F was predicted. The DTS fiber values were also verified with a calibrated wireline temperature survey and show a close match in profile to the installed fiber. The profile shows conductive temperature conditions as expected, with the exception of a 7°F reversal from 6620 to 6690 ft MD which correlates with a mud loss zone encountered in the well where 43 bbls total were lost from 6630 to 6640 ft MD.

The phyllite basement contact prediction for 34A-22 was 3,750 ft MD with an error range of 3,500-4,000 ft MD, based on the updated model following completion of 73-22. Upon drilling 34A-22, the phyllite basement contact was observed at 3500 ft MD, or the shallow edge of the predicted error bars. Interestingly, that indicates a dip for the basement contact of 29° between 34A-22 and 34-23, which was the originally modeled dip assumption before drilling 73-22. The reality is that there is likely variation/undulation of the contact dip within the fault block, which is why 5°of variation was assumed on the predicted depth range and underscores the value of having error bars on the contact predictions. This natural undulation in the overall contact dip is incorporated into the 3D model with ties to the well observations.

Three potential faults were predicted in 34A-22, at 670 ft MD (South Fault), 6,140 ft MD (SW Range Front), and 11,250 ft MD (55-15 fault). Indications of the South Fault were not observed, which could be due to its position within unconsolidated sediments where it was predicted to intersect the well. Faults are often only expressed as open fractures where they have hard formation to keep them open, and this fault may only be expressed deeper where it intersects and offsets the phyllite basement or more indurated sediments. The SW Range Front fault was also not observed within the predicted depth range; however, it was classified as low probability based on observations in 73-22 where only minor clay and calcite indicators were seen without significant mud losses. A small 43 bbl mud loss was encountered

in 34A-22 from 6630 to 6640 ft MD, which may have been caused by the SW Range Front fault with a slightly steeper dip than modeled. This loss zone only lasted for 10 ft of drilling before it was sealed off by 2-5mm cuttings, indicating that it was likely expressed as a small aperture (<5mm) fracture in the wellbore. This loss zone could alternatively be unrelated to the SW Range Front fault, and instead been related to stratigraphic permeability within the formation or foliations. Finally, the 55-15 fault was not observed, however the total depth of 34A-22 (11,220 ft MD) did not reach the full predicted depth range of that fault (11,250 +/- 150 ft MD).

4.3 Production Well 34-22

The temperature profile for 34-22 was expected to be nearly identical to 34A-22 in the vertical portions of the wells, since they are both located on the same pad ~150 ft apart. In the lateral portions, based on the updated 3D temperature model using the results from 73-22 and 34A-22, 34-22 was expected to be ~5°F warmer on average than 34A-22 due to 34-22 being 200-300 ft further north, which places the well closer to the convective geothermal system and source of hot deeply circulating fluids for the system. This translates to a prediction of 372°F at the heel (8000 ft MD) and 343°F at the toe (11,225 ft MD) for 34-22. DTS fiber temperatures in 34-22 indeed showed a profile identical to 34A-22 in the vertical section and warmer by a few degrees in the lateral. Although the temperature of 34-22 has not been recorded at ~5°F higher than in 34A-22, as predicted, at the time of the latest fiber reading the well was still heating up and not fully equilibrated (Figure 6).

Significant de-risking of faults for 34-22 occurred with the drilling of 34A-22 just 150 ft to the east. Potential fault candidates (such as the South Fault) were eliminated as hazards based on the drilling results of 34A-22 which did not see the structure. Two minor faults were still predicted in 34-22 at 6400 ft MD +/- 100 ft MD (SW Range Front), and 11,000 ft MD +/- 200 ft MD (55-15 fault). The SW - Range Front fault caused a small 43 bbl mud loss in the previous 34A-22 well that lasted for 10 ft of drilling before it was sealed off by 2-5mm cuttings, indicating that it was likely expressed as a small aperture (<5mm) fracture in the wellbore. Where it was expected in 34-22, a minor loss of 10 bbl/hr was encountered at 6,365 ft MD, which was above the background of 3-5 bbl/hr. This increase in losses in 34-22 was small but insignificant as a hazard; however, it could be indicative of the presence of a minor natural fracture. The 55-15 fault was not observed in either 34A-22 or 34-22; however, both wells were completed to a total depth shorter than the total depth range within that the fault was predicted to occur.

During Fervo's stimulation of 34A-22, a distinctive 100 mesh size proppant sand was injected into 34A-22 and the fracture network created during stimulation. The 100 mesh proppant was composed of sub-rounded pure quartz sand grains with the strict 100 mesh filter size and a bright yellow-orange oxidized coloration. No mineralogies match these characteristics in the natural formation, and no quartz sands matching the proppant were observed in the prior wells. Since well 34-22 was drilled after the stimulation and proppant injection into 34A-22, close attention was paid to the 34-22 cuttings while drilling to detect the proppant, with hand samples of un-injected proppant sitting beside the cuttings microscope for direct comparison. 14 zones of proppant were indeed detected in the 34-22 cuttings (orange zones in Figure 7), proving direct evidence that Fervo's stimulated fracture network reached across the field between the two well laterals. In most of these cases, the detections included 2-3 grains in a single 10-ft cuttings sample interval. Because proppant concentrations are observed to be quite low at this distance from 34A-22, the absence of detections in the other intervals of the well are not thought to be evidence of the absence of proppant or stimulated fractures in those areas.

4.4 Intrusives

Before the drilling of Fervo wells at Blue Mountain, the prevalence of intrusive diorite and granodiorite dikes/sills across all wells at Blue Mountain was analyzed and 17,785 ft of intrusives were found within 93,436 ft of Mesozoic basement formation, providing an apparent intrusive ratio of 19% as percent of basement. Another observation made across this dataset was that the diorite and granodiorite dikes/sills are almost never found in the shallowest 3000 ft of phyllite below the contact with sediments. As Fervo drilled 73-22, 34A-22, and 34-22 that trend held and intrusives were not observed until at least 3000 ft below the phyllite basement contact. In well 73-22, 1659 ft of intrusives were observed in the basement that was drilled from 2,430-8,009 ft MD, representing a ratio of 30% intrusives to phyllite. Only looking at the 8-3/4 in section of the well from 5,009-8,009 ft MD which in reality is the only portion of the basement where the dikes/sills exist, an intrusive ratio of 55% is obtained. In 34A-22 1,723 ft of dikes/sills were observed in the basement that was drilled from 3,500-11,220 ft, resulting in an intrusive to phyllite ratio of 22%. Again, if we only look at the 9-7/8 in section from 7,969-11,220 ft MD where the dikes/sills predominantly exist, 43% of the basement is comprised of intrusives. The prevalence of dikes/sills in 34-22 was very slightly lower than in 34A-22, with 1,310 ft of dikes within the 9-7/8 in section of 34-22 providing am intrusive ratio of 40% (green and blue zones in Figure 7). Diorite and granodiorite dikes mapped at the surface of Blue Mountain and to the south at the Eugene Mountains are expressed mostly as low-angle bedding-parallel sills exploiting bedding weaknesses in the phyllite (Thole and Prihar, 1998). Image log data from 34-22 also suggest contacts between the intrusives and metamorphic basement are oriented north to northeast and dip west, parallel to bedding (see Section 5). Efforts at modeling the intrusive contacts between wells have proven difficult due to the large number of features, high variation in thicknesses, and laterally discontinuous nature of the sills.

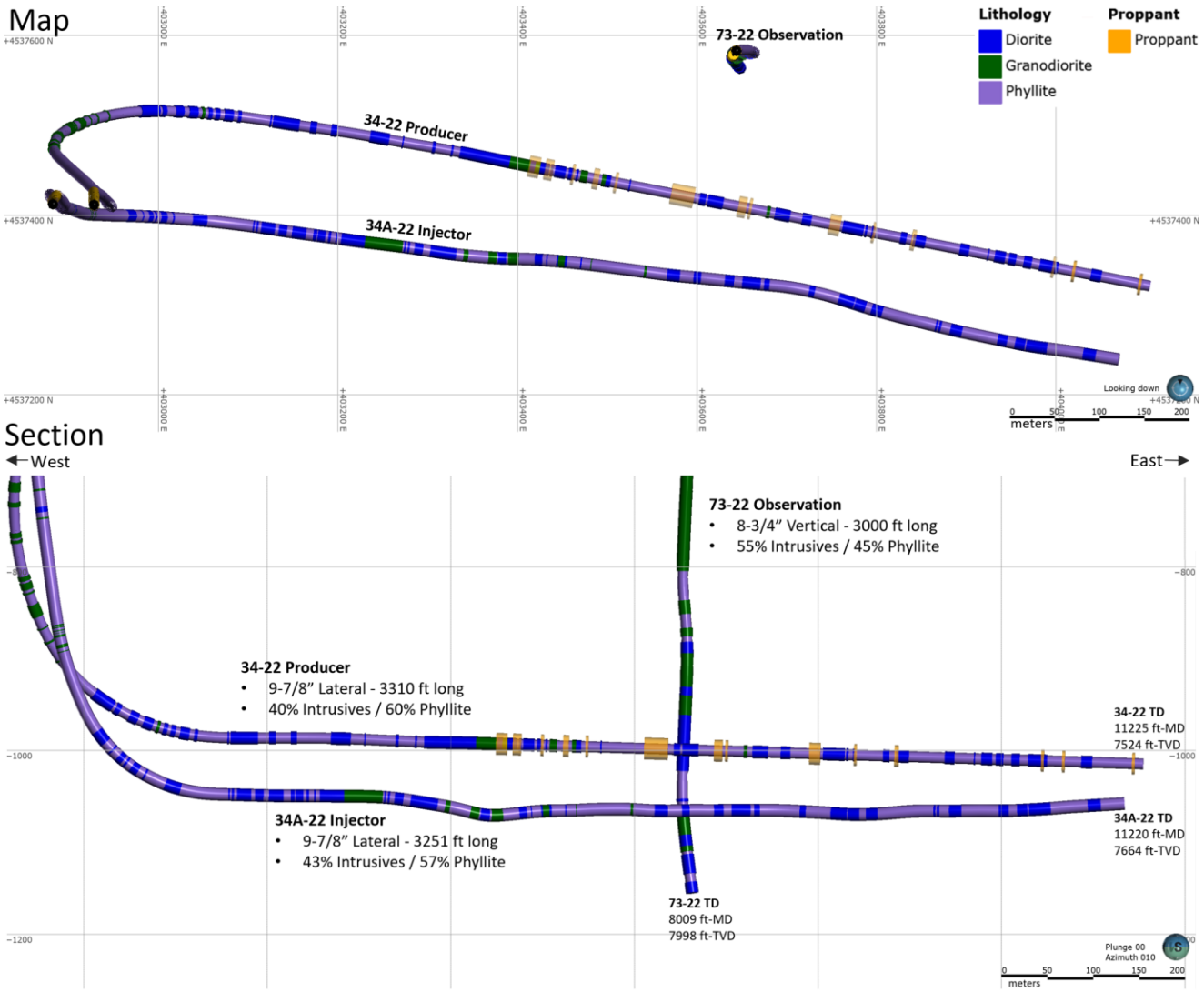

Figure 7: Lithologies and proppant detections plotted along the wellpaths for Fervo wells 34-22, 34A-22, and 73-22.

5. STATE OF STRESS

Prior to Fervo's 2022 drilling campaign, there were four existing wells with image log data at Blue Mountain, which were reviewed in Geologica (2020). All the logs were collected in the phyllite basement formation. From NE to SW, the Geologica report found that drilling-induced fractures (DIFs) at Blue Mountain have an average azimuth of 010.3° in 58-11, 009.5° in 44-14, 021.4° in 26A-14, and 037.6° in 55-15 (Figure 8). Stress inversion calculations from ground fault surface measurements collected in 2020 indicate SH_{max} oriented 019° and within the range of the well data. The trend of distribution of DIFs in these wells showed a steady progression of clockwise rotation of SH_{max} along a NE-SW trend, starting from 58-11 and extending through 55-15. The apparent rotation may be due to local variations in stress occurring in the accommodation zone between the NW- and NE-striking faults at Blue Mountain. Stress rotations have been documented in relay ramps in step-overs associated with extensional fault regimes globally (Fodor, 2007). Earthquakes induce temporal changes in magnitude (e.g., Siler et al., 2018) and orientation of the stress field (e.g., Hardebeck and Okada, 2018). Localized vertical axis stress rotation has recently been interpreted for the upflow of the Star Peak geothermal resource (Fercho et al., 2020). Prior to Fervo's drilling campaign, the largest gap in stress field data was that there was no image log data for wells on the south side of the reservoir.

Image logs were collected in two portions of Fervo well 73-22, the 12-1/4 in hole section from 2,615-5,002 ft MD and the 8-3/4 in hole section from 4,952-7,988 ft MD. Log quality in the 12-1/4 in section was low, and DIFs were either not observable or not present in that portion of the well. In the 8-3/4 in hole section, however, there were over 900 well-developed DIFs observed though nearly the entire interval (Figure 9). The DIFs in 73-22 were clustered with an average orientation and resulting SH_{max} orientation of 59.5° northeast. This shows a continued trend of clockwise rotation to the SW, although to a larger degree than was expected (Figure 8). As 73-22 is located approximately at the midpoint of Fervo's planned lateral wells, we are used this SH_{max} orientation to determine the optimal orientation of

the lateral sections of those wells balanced against the temperature model. Further variation of the stress field may occur along the lateral wells at both the heel and the toe, but we expect it to still be within the range of this SH_{max} orientations observed throughout the field. Borehole breakouts, which typically occur 90° from the SH_{max} orientation and represent the orientation of SH_{min}, were only observed in a small interval of 73-22 from 7,510-7,574 ft MD and had an average azimuth orientation of 160° (southeast). Bedding/banding of the phyllite was observed to predominantly dip to the NW with a 300° average dip azimuth with a smaller significant population dipping to the SW with a 255° average dip azimuth. Natural fractures tightly cluster and dip NW with an average azimuth of 300°.

A resistivity image log was also successfully collected in the horizontal portion of Fervo's 34-22 well. In summary, features interpreted from the image log can be generally split into three groups: (1) natural features that dominantly strike north-south and are most likely associated with the rock fabric, (2) natural features that dominantly strike northwest to north-northwest and are most likely associated with fault zones, and (3) drilling induced damage generated by the hoop stresses at the borehole wall. The 34-22 image yielded an unusually high number of electrically conductive features (Figure 10). In summary, these data indicate that the contacts between the intrusive dikes and metamorphic basement are likely to be oriented north to northeast and dip west. Features confidently identified as internal bedding strike north to northeast and dip west. Electrically conductive natural fractures observed in the 34-22 image log have two distinct populations, a NNE striking, west-dipping population and a smaller conjugate NNW striking, east-dipping population (Figure 11). The west dipping population has a mean dip azimuth of 279.4° with a dip of 67.1° NW out of 851 picks. The east dipping population has a mean dip azimuth of 80.3° with a mean dip of 72.3° E out of 326 picks.

Drilling induced damage in 34-22 includes axial and en echelon tensile fractures and borehole breakout. These features on the borehole wall are a consequence of hoop stresses. Overall, axial tensile fractures and the center-point of en echelon tensile fractures formed 150 – 160° from the high-side of the borehole (i.e., just before the lowest point), with some rotations that likely relate to fault zones. Tensile fractures at the high side are not resolved in the micro-resistivity image because of poor pad contact with the borehole wall. The acoustic image also does not resolve the high-side tensile fractures, likely because the tool was not central in the well. Borehole breakout formed on either side of the 34-22 borehole at a wide range or orientations, consistent with a horizontal well drilled in a normal faulting setting.

Exploratory forward model scenarios were used to determine the distribution of DI Damage on an inclined borehole were constructed using the system of equations outlined by Peska and Zoback (1995). This method projects the tectonic stress tensor (orientation and magnitude) onto the borehole wall to calculate the hoop stresses and, subsequently, the characteristics of the resulting DI Damage. These results indicate that the stress field determined from data in 34-22 may be characterized by SH_{max} of ~020° and the stress conditions may be transitional to strike-slip. This is consistent with stress modeling of fault surface data, which indicated SH_{max} azimuth of 019° (NNW) and a Mohr's circle stress ratio R value calculation of 0.71 which indicates a transtensional regime.

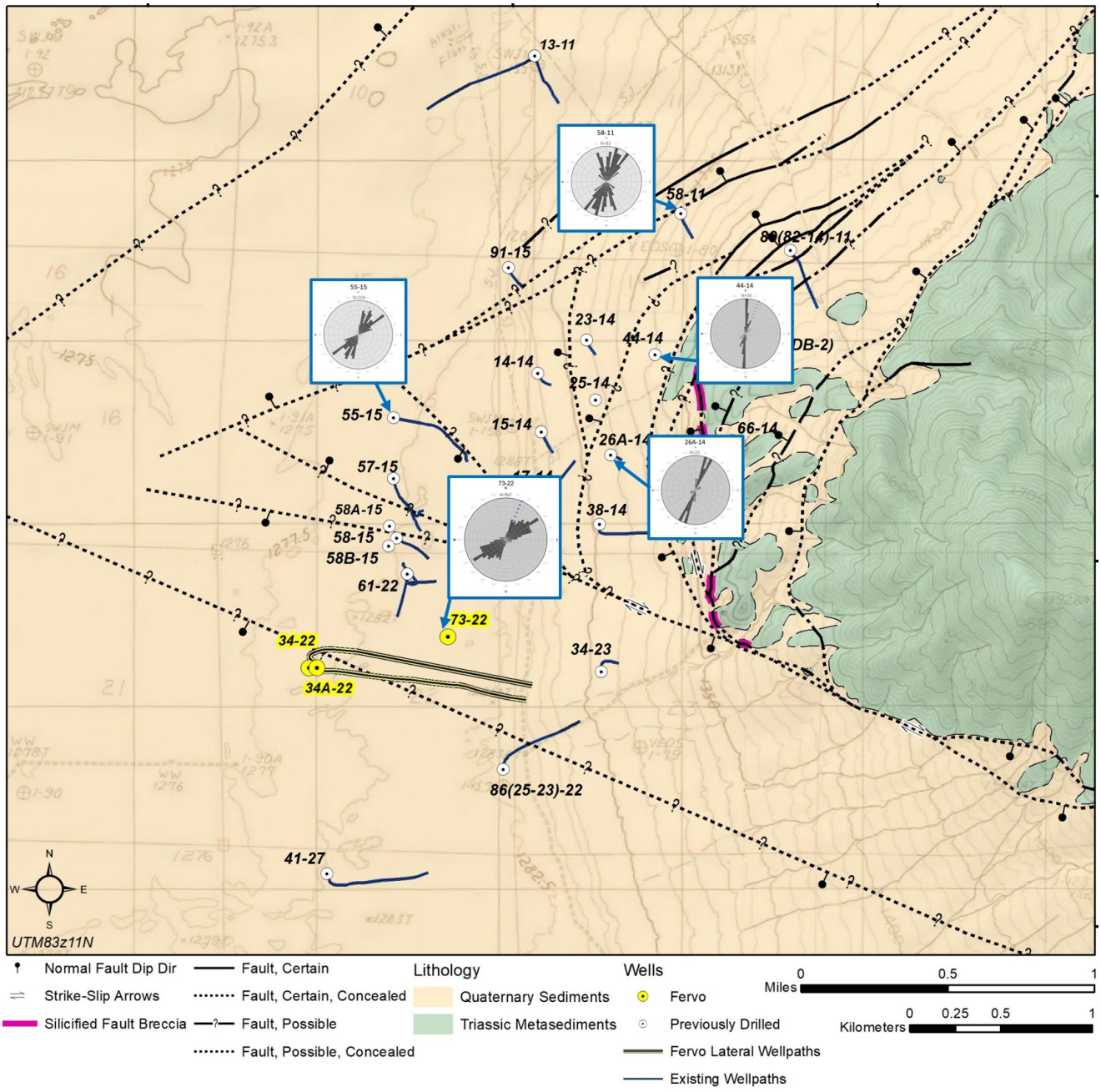

Figure 8: Map and rose diagrams showing the locations and orientations of drilling-induced fractures at Blue Mountain, 73-22 DIFs are shown trending NE at the south end of the field.

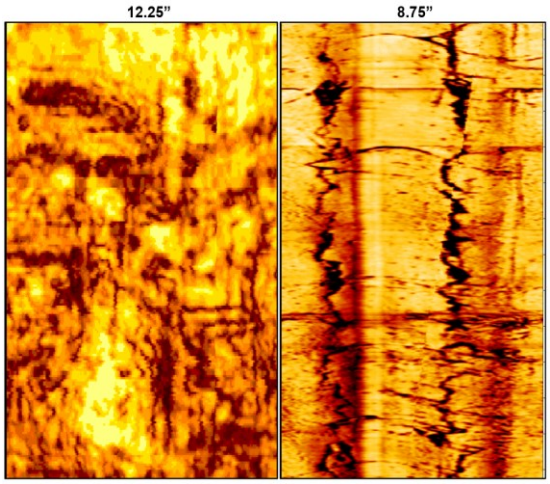

Figure 9: Example sections of the acoustic image logs collected in Fervo well 73-22 in the 12-1/4 in hole section (left) and the 8-3/4 in hole section (right). Well-developed drilling induced fractures can be seen in the example from the 8-3/4 in hole section.

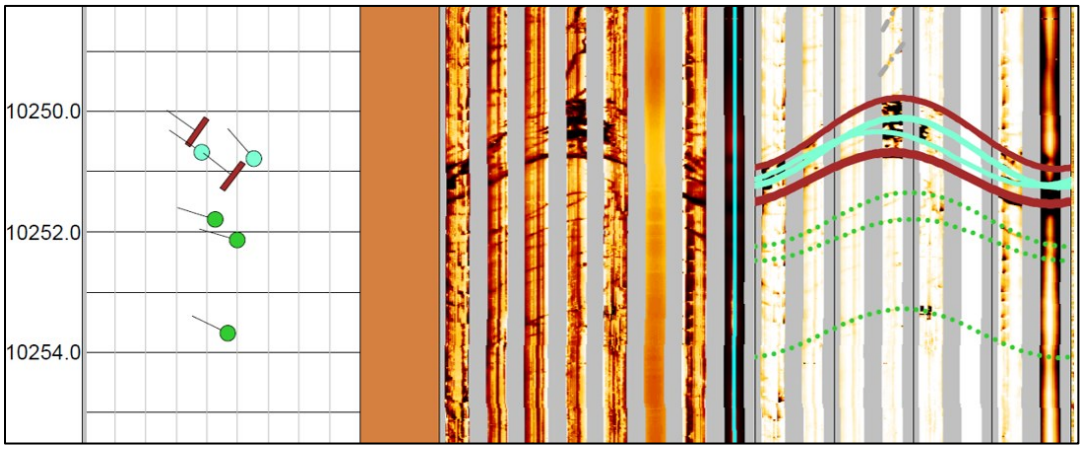

Figure 10: Example section of the high quality resistivity image log collected in the horizontal portion of Fervo well 34-22 showing foliations and composite features.

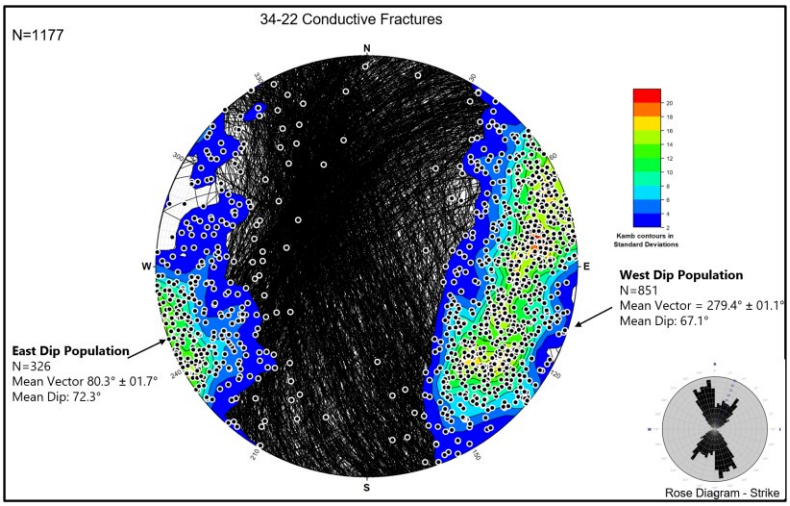

Figure 11: Stereonet and rose diagram showing the orientations of all electrically conductive fractures from the Fervo well 34-22 resistivity image log.

6. HEAT-IN-PLACE MODELING

As a first step in characterizing the resource potential of a horizontal well geothermal development strategy, we performed a heat-in-place analysis for the Fervo doublet horizontal well system at Blue Mountain. This is a useful method that can be used to set bounds on the power capacity of the system prior to production testing. The results of the heat-in-place analysis can be used to evaluate the economic viability of the project.

Heat in place can be calculated with the following equation (Grant and Bixley, 2011):

$$H_{\text{tot}} = \int \rho c (T - T_0) dV, \tag{1}$$

where H_{tot} is the total thermal energy originally in place, ρ is the reservoir rock density, c is the reservoir rock heat capacity, T is the reservoir rock temperature, T_0 is a reference temperature (taken as the geothermal brine temperature at the outlet of the power plant heat exchanger), and V is the reservoir volume. The thermal energy actually recoverable is controlled by the thermal recovery factor, which can depend on the well pattern, the stimulation efficiency, the geometry of the stimulated reservoir volume, the thermal diffusivity of the rock, the reservoir management strategy, and other geologic and operational factors. The recoverable heat in place is then:

$$H_{\text{recov}} = r \int \rho c (T - T_0) dV, \tag{2}$$

where r is the thermal recovery factor. For the scenario of geothermal electric power production considered here, the electrical energy that can be generated from the resource can then be calculated as:

$$E = \eta r \int \rho c (T - T_0) dV, \tag{3}$$

where η is the thermal-to-electric conversion efficiency of the binary power plant facility. We can then calculate the power capacity of the system (averaged over the lifetime of the facility) as:

$$P = \frac{E}{\Delta t}, \tag{4}$$

where Δt is the lifetime of the facility.

The heat-in-place for Fervo's project area at Blue Mountain was calculated using Ferov's three-dimensional geologic model and temperature distribution, where the subsurface was discretized into a Cartesian mesh with uniform grid block size. Grid block volumes of 10 x 10 x10 m was selected for the model, giving each block a volume of 1000 m^3. Values for heat capacity were populated assuming the average heat capacities of phyllite and of diorite (Waples and Waples, 2004). Values for density of the phyllite and diorite dikes were obtained from Fervo's analysis of quad combo logs collected in well 73-22. The proportion of phyllite to diorite by length in well 34A-22 was 57% and in well 34-22 was 60%, therefore an average proportion of phyllite to diorite of 58.5% was assumed for the bulk volume of rock between and immediately surrounding the wells. Applying these proportions to the heat capacity and density values derived for the phyllite and diorite, we obtained an effective density of 2,782 kg/m^3 and a heat capacity of 0.77 kJ/kg/°C for the bulk intruded phyllite formation (Table 1). Finally, the reference temperature was taken as 75 °C based on the average reinjection fluid temperature for the Blue Mountain wellfield.

Table 1: Heat capacity and density values calculated for heat-in-place models.

Rock Type	Heat Capacity (kJ/kg/K)	Density (kg/m^3)	Source
Phyllite	0.76	2720	73-22 Quad Combo Log; Waples and Waples (2004)
Diorite	0.79	2870	73-22 Quad Combo Log; Waples and Waples (2004)
Intruded Phyllite (59% Phyllite / 41% Diorite)	0.77	2782	Weighted average based on proportional lithologies observed along the laterals

The heat-in place model created for this study covers the extent of stimulated reservoir volume created by Fervo's multistage stimulation of well 34A-22 and has dimensions of 1030 m x 540 m x 240 m. Injection Well 34A-22 was stimulated with a 16-stage plug-and-perf hydraulic stimulation treatment with proppant, in which a total of approximately 267,000 bbl (11.2 million gal) of fluid and 7.3 million lbs of sand proppant were pumped. The stimulated reservoir volume geometry was characterized using several independent reservoir diagnostics approaches, including microseismic monitoring, fiber optic strain sensing, pressure transient analysis, and offset well pressure monitoring (Norbeck et al., 2023). Several points of evidence lead to these fracture extents, including the extent of microseismic events and strain data deriving fracture half-length and half-height from DAS fiber installed in 34A-22, 34-22, and 73-22 (Figure 12).

The heat-in-place model for Fervo's stimulated reservoir volume computes a total thermal energy originally in place (H_{tot}) of 3.04x10^{13} kJ using the above inputs. Based on analog geothermal systems, thermal recovery factors can range from about 20% to 50%. Fervo has performed computational reservoir modeling and found a similar range of recovery factors depending on well spacing, stimulation treatment design, and geologic factors. Therefore, for this analysis we assume a thermal recovery factor (r) of 35%. The thermal-to-electric conversion efficiency (η) was assumed to be 15% based on the observed plant efficiency. Typically, geothermal power facilities are designed for a useful life of 15 to 30 years, however, given the infill and repower nature of this project, the system was designed for a useful project life (Δt) of 10 years.

Under these assumptions, we found the effective average power capacity of Fervo's horizontal well doublet system to be 5.1 MW. This is consistent with the power output of a geothermal well producing at approximately 80 kg/s at a temperature of 350 – 375 °F (the target well performance of the Fervo system), given the power conversion efficiency of the Blue Mountain facility. Therefore, we can conclude that the stimulated reservoir volume created during the 34A-22 treatment is sufficiently large to meet the reservoir performance requirements for this project.

For this heat-in-place analysis, we used only the SRV from the stimulation treatment on one well (Injection Well 34A-22). Prior to production testing, Production Well 34-22 will also be stimulated, likely adding significant reservoir volume and fracture surface area. In addition, due to the first-of-a-kind nature of this horizontal drilling program, the productive lateral length of each well was limited to about 1000 m. In future projects, it will be possible to drill longer laterals that can increase the reservoir volume. In addition, through additional field trials focused on completion design optimization, the thermal recovery factors for these systems may be improved. Therefore, 5 MW per production well may be a lower bound for this type of well design and reservoir management strategy.

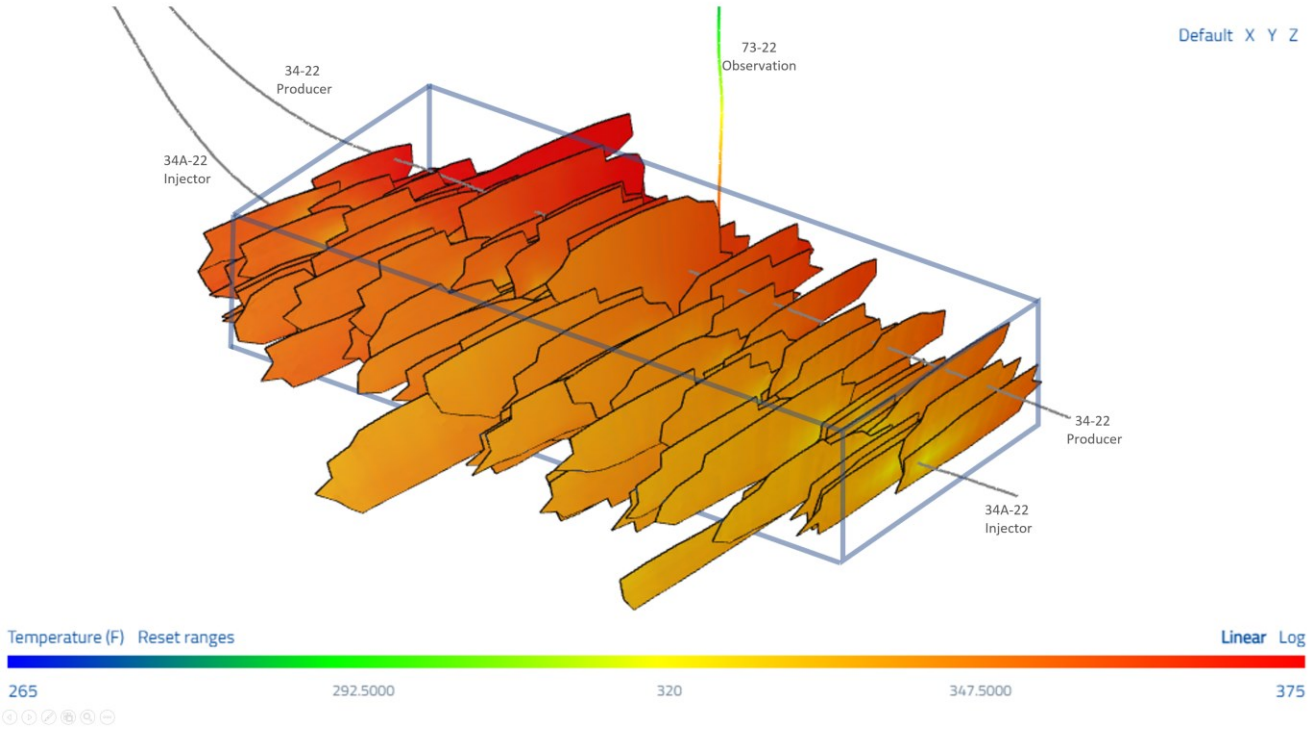

Figure 12: Extents of heat-in place model (grey box) within Fervo's stimulated fracture geometry based on stimulation history matching of well 34A-22.

7. CONCLUSIONS

In this paper, we describe the results from a nearfield enhanced geothermal system project targeting a low permeability reservoir compartment adjacent to the Blue Mountain hydrothermal system at a depth of 7000-8000 ft (2.1 to 2.5 km). Three deep wells were successfully drilled by Fervo Energy at Blue Mountain, including the first two known high-temperature geothermal horizonal wells drilled metamorphic and igneous lithologies. We developed a reservoir conceptual model using offset well data, geologic mapping, and geophysical surveys to design the drilling program and inform the stimulation treatment design. The as-drilled lithology and measured equilibrated temperatures matched the model predictions closely, confirming the value of developing this style of project in a nearfield hydrothermal setting. Drilling induced fractures from image logs and stress modeling indicate an SH_{max} aligned to the NNE and informed the optimal orientation for the lateral trajectories of the horizontal wells 34A-22 and 34-22. Fervo well 34A-22 was impermeable prior to stimulation and had proppant injected during stimulation which was detected 300-400 ft away while drilling the lateral portion of 34-22, providing direct geologic evidence of the successful creation of a new hydraulicly stimulated fracture network. Heat-in-place estimates confirm that the stimulated reservoir volume created from the stimulation treatment in well 34A-22 was sufficiently large to enable approximately 5 MW of electric power production over a 10-year project life, consistent with the target well performance for this project.

The successful completion of this project indicates that no technical barriers exist to developing horizontal drilling and completions programs in high-temperature and complex hard rock settings. The reservoir performance results described for this first-of-a-kind project demonstrate that nearfield EGS projects can be developed economically today and show a clear pathway toward further improvements in project economics with reasonable advances in drilling performance, stimulation treatment effectiveness, and reservoir management strategies.

ACKNOWLEDGEMENTS

Funding provided by DOE EERE Geothermal Technologies Office to Utah FORGE and the University of Utah under Project DE-EE0007080 Enhanced Geothermal System Concept Testing and Development at the Milford City, Utah Frontier Observatory for Research in Geothermal Energy (Utah FORGE) site.

REFERENCES

Coolbaugh, M., Zehner, R., Kreemer, C., Blackwell, D., and Oppliger, G.: A Map of Geothermal Potential for the Great Basin, USA: Recognition of Multiple Geothermal Environments, GRC Transactions, Vol. 29 (2005).

Faulds, N.H., and Hinz, N.H.: Favorable tectonic and structural settings of geothermal settings in the Great Basin Region, western USA: Proxies for discovering blind geothermal systems: Proceedings, World Geothermal Congress 2015, Melbourne, Australia, 6 p (2015).

Fercho, S; Hinz, N; Casteel, J; Turk, J: Analysis of Natural and Drilling Induced Fractures from Newly Acquired Borehole Image Logs at the Star Peak Geothermal Field, NV: Implications for Localized Stress Field Rotation Within a Normal Fault Step-Over. Geothermal Resources Council Transactions, 44, (2020).

Fodor, L.I.: Segment Linkage and the State of Stress in Transtensional Transfer Zones: Field Examples From The Pannonian Basin. Geological Society, London, Spec. Pub, v. 290, 417-431(2007).

Geologica Geothermal Group: Blue Mountain 2020 Conceptual Model Final Report. Unpublished Technical Report (2020).

Grant, M.A. and Bixley, P.F.: Geothermal Reservoir Engineering. Academic Press, 2nd ed., Oxford, (2011).

Hardebeck, J. L., and Okada, T.: Temporal Stress Changes Caused By Earthquakes: A review. Journal of Geophysical Research: Solid Earth, 123, 1350–1365. (2018).

Norbeck, J., Gradl, C., Agarwal, S., Dadi, S., Fercho, S., Lang, C., McConville, E., Titov, A., Voller, K., Woitt, M., and Latimer, T.: Drilling and Completions Engineering Review of a Horizontal Geothermal Drilling Program and a Multistage Hydraulic Stimulation Treatment Design at Blue Mountain, Nevada. Proceedings, 48th Workshop on Geothermal Reservoir Engineering, Stanford University, Stanford, CA (2023).

Niggemann, K., Fairbank, B.; Petty, S.,: Deep Blue No.2 -A Resource in the Making at Blue Mountain, GRC Transactions, Vol. 29 (2005).

Peska, P. and Zoback, M.: Compressive and tensile failure of inclined well bores and determination of in situ stress and rock strength. Journal of Geophysical Research 100:B7, p. 12791 – 12811, (1995).

Siler, D.L., Hinz, N.H., Faulds, J.E.: Stress Concentrations At Structural Discontinuities In Active Fault Zones In The Western United States: Implications for permeability and fluid flow in geothermal field. Geological Society of America Bulletin (2018).

Szybinski, Z.A.: Structural Setting of the Blue Mountain Geothermal Project Area, Humboldt County, Nevada, unpublished report for Nevada Geothermal Power Inc, (2005).

Thole, R H. and Prihar, D W.: Geologic Map Of The Eugene Mountains, Northwestern Nevada. Nevada Bureau of Mines And Geology Map 115 (1998).

Waples, D. W., and Waples, J. S.: A Review and Evaluation of Specific Heat Capacities of Rocks, Minerals, and Subsurface Fluids. Part 1: Minerals and Nonporous Rocks. Natural Resources Research, Vol. 13, No. 2, (2004).